J. Phys. Chem. A **2003,** *107,* 1377−1383

First-Principle Study of Molecular Springs under Shear Deformation

Hong Seok Kang*,† and J. Bernholc‡

College of Natural Science, Jeonju University, Chonju, Chonbuk 560-759, Republic of Korea, and Department of Physics, North Carolina State University, Raleigh, North Carolina 27695-8202

Received: August 10, 2002; In Final Form: November 28, 2002

Recently synthesized tunable molecular springs are investigated theoretically using massively parallel density functional simulations with the generalized gradient approximation. The springs are salts of organosilver complexes that crystallize in structures with monoclinic symmetry. For springs with NO_3^- (N-spring) and ClO_4^- (Cl-spring) ions as negative balancers, we are able to refine their X-ray structures. Our calculations of total energies as functions of the nonorthogonal lattice angle β correctly reproduce the experimental equilibrium values of the angle for both the N- and Cl-springs. For the N-spring, our calculations reveal that the nitrate ions undergo concerted propeller rotations in the clockwise direction as the angle increases by 10° around the experimental value. For the Cl-spring, the rotations of chlorate ions are more enhanced in a limited range of the β angle, but they move in the counterclockwise direction. For the N-spring, the potential energy curve is symmetric and the shear modulus is about 0.01TPa. Calculations of the electronic density of states show that both springs are semiconductors.

Introduction

Molecular springs with tunable helical pitches were synthesized recently.[1] At the room temperature, these organometallic salts form monoclinic crystals whose unit cell contains two helical strands of opposite handiness. Simply suspending the crystal in a solution of another negative balancer X results in a complete exchange of negative ions, leading to a large change in the helical pitch, up to nearly 30%. This structural flexibility in the helical morphology could lead to applications in molecular devices and biological systems. Since the physicochemical properties are closely related to the atomic structure, understanding the structural changes occurring during the change of the balancers and/or other changes in the experimental conditions will be useful in designing practically valuable variants with physical properties appropriate for various molecular devices.

With the development of powerful computers, density functional theory (DFT)[2] combined with pseudopotential (PP) theory of electron−ion interaction,[3] has become an increasingly important tool in physics, chemistry, and biology for the investigation of systems that consist of large number of atoms. In this work, we use the so-called real multigrid method, which allows for particularly efficient calculations for large systems and also parallelizes effectively on massively parallel supercomputers.[4] Equipped with these theoretical tools, the present work is the first step toward the understanding of physicochemical properties of the molecular springs from first-principles calculations. In particular, we investigate the structural changes due to shear deformation, by calculating the total energy of optimized structures at various lattice angles. We focus on two kinds of springs, the "N-spring" and the "Cl-spring", which are characterized by $X = NO_3^-$ and ClO_4^-, respectively. They exhibit large (=25%) difference in the helical pitch.

Theoretical Method

The calculations were carried out on massively parallel IBM-SP and CRAY-T3E supercomputers. The one-electron Kohn−Sham (KS) equations were solved at a dense grid of points of real-space, using nonlocal pseudopotentials (PP) in Kleinman and Bylander's separable form[5] to describe the effects of core electrons. The pseudopotentials were generated by the Troullier−Martins scheme[6] using the electronic configuration of Bachelet, Hamann, and Schlüter.[7] The exchange-correlation (XC) functionals were calculated within the generalized gradient approximation (GGA), using the Perdew, Burke, and Ernzerhof (PBE)[8] parametization.

The Kohn−Sham equations were solved iteratively, employing the multigrid method to accelerate convergence.[9] This method exploits the fact that iterations quickly reduce error components that are oscillatory on the scale of the grid, while the long wavelength components converge only slowly. After a convergence slowdown is observed, we recursively transfer the approximate solution to a coarsened grid, where the error becomes oscillatory, and iterate there. The coarsened solutions are then transferred back to the finer grids, using a few fine-scale iterations to reduce high frequency errors introduced by interpolation. At the finest levels, the grid resolutions corresponded to cutoff energies of 86.1 and 70.6 Ryd for the N- and Cl-springs, respectively. Our real-space formulation does not rely on any kind of localized orbitals, the only approximation being the grid discretization. The reliability and usefulness of the multigrid method in the electronic structure context have been proven by applications to a variety of physical problems, including studies of mechanical and quantum transport properties of carbon nanotubes[10] and of structures and optical anisotropies of semiconductor surfaces.[11] In all of the above work it was possible to use a fourth-order "Mehrstellen" discretization of the KS equation, which discretizes the entire differential equation, rather than just the kinetic energy, and is very compact. Unfortunately, we have so far derived the Mehrstellen discretization only for cubic, orthorhombic, or hexagonal primitive cells. Since the crystal structure of the molecular springs is monoclinic,

---

* To whom correspondence should be addressed. E-mail: hsk@www.jeonju.ac.kr. E-mail: hsk@nemo.physics.ncsu.edu.

† Jeonju University.

‡ North Carolina State University.

10.1021/jp0267353 CCC: $25.00

TABLE 1: Bond Lengths (in Angstroms), Bond Angles, and Other Geometrical Parameters for the N-Spring[a]

	EXP	MP2	JUNG	LDA+0	PBE−5	PBE+0	PBE+5
l(C−H)	1.084[b]		0.93(1)	1.09(1)	1.08(1)	1.08(1)	1.08(1)
l(Ag−Ag)[c]			3.35(0)	3.18(1)	3.21(1)	3.17(1)	3.17(1)
l(Ag−N)		2.241[d]	2.14(1)	2.15(1)	2.15(1)	2.16(1)	2.13(1)
l(N−O)	1.24[e] 1.26[f]	1.273[g]	1.22(1)	1.26(1)	1.27(1)	1.27(1)	1.27(1)
l(N−N)[h]			4.27(0)	4.29(1)	4.28(1)	4.30(1)	4.25(1)
θ(N−N-X)[i]			76.1(0)	76.0(1)	75.2(1)	76.0(1)	76.2(1)
θ(N−Ag−N)[j]		180.0[d]	173.1(0)	169.6(4)	170.2(5)	169.7(4)	169.5(6)
θ(ion-ion-X)[k]			62.4(0)	62.7(2)	62.5(1)	62.8(2)	64.2(3)
χ[l]			48.2(0)	47.7(1)	47.5(1)	46.6(1)	47.2(1)

[a] EXP denotes values taken from experimental data, and MP2 represents data calculated in this work using the MP2 method in the GAUSSIAN98 program. JUNG denotes Jung et al's X-ray data at the lattice angle $\beta = 99.04$. Other data were obtained in this work after structure optimization. LDA is based on the LDA parametrization of Perdew and Zunger, while PBE denotes the GGA parametrization of ref 8. Suffixes −5, +0, and +5 correspond to $\beta = 94.04°$, 99.04°, and 104.04°, respectively. Values in parentheses denote the standard deviations in the last decimal place. [b] Experimental data taken from ref 14. [c] Interatomic distance between proximal silver atoms not belonging to the same helical strand. [d] Value obtained in this work from a MP2/LANL2DZ calculation for the $Ag(NH_3)^{2}+$ ion using the GAUSSIAN98 program. Discrepancy of this bond length from other values in the table can possibly reflect the inaccuracy of the calculation with LANL2DZ bases set for Ag compounds. [e] Experimental data taken from ref 20. [f] Value quoted in ref 21. [g] Value obtained in this work from a MP2/6-31++G* calculation for NO_3^- ion using the GAUSSIAN98 program. [h] Interatomic distance between nitrogen atoms belonging to the same N−Ag−N motif. [i] Angle that the N→N vector between nitrogen atoms in the same N−Ag−N motif makes with the X axis. [j] Bond angle between corresponding atoms in the same N−Ag−N motif. [k] Angle that the vector $NO_3^- \rightarrow NO_3^-$ between nitrate ions in the same helical strand makes with the X axis. [l] Angle that two N→N vectors in the same helical strand make with respect to each other.

we developed procedures for solving the KS equation that are based on eighth order finite difference dicretization on a monoclinic grid, using 25 and 33 grid points for Laplacians and the gradients of the wavefunctions. Optimization of the atomic positions was achieved by relaxing in the direction of the Hellmann−Feynman forces[12] for several tens of steps, until the average force was less than 0.0005 Hartree/a_0, where a_0 is the Bohr radius.

Only the Γ-point was included in the k-space sampling unless specified, since the unit cell is so large that the difference in the total energy is less than 0.001 Hartree for calculations with 1 and 2 k-points in the Brillouin zone along the helical axis, the direction of the shortest lattice parameter. Most of our results have been calculated with the PBE XC functional (PBE-OPT). Since the local-density approximation (LDA) usually predicts bond lengths that are slightly shorter than the experimental values while the GGA behaves oppositely, the LDA calculations help to assess the reliability of our theoretical results. This is especially the case when there are large discrepancies between the experimental data and the PBE-OPT results. Our LDA calculations are based on the exchange-correlation parametrization due to Perdew and Zunger.[13] Similarly to the case of PBE-OPT, LDA-OPT denotes a structure optimized using LDA forces.

Results

Refinement of the X-ray Structure: We briefly describe the structural features of the spring that are relevant to our discussion. Important structural motives are: (i) coordination of Ag(I) with nitrogen atoms through a N−Ag−N bond and (ii) Py_2O, in which two 3,3′-oxybispyridines (Py) are connected to an oxygen atom. One helical turn consists of two units of alternating N−Ag−N and Py_2O motifs. Negative balancers X form two columns along the axis of the oblong helix. In our work, the Cartesian coordinate system is defined in such a way that the positive X axis is parallel to the lattice vector **c**, and the Z axis (=helical axis) is parallel to **b** of the $P2_1/c$ space group. The primitive cells contain 104 and 108 atoms for the N- and Cl-springs, respectively. The lattice vector **a** lies in the XY plane and makes an angle β with the X axis. In Jung et al's X-ray data (JUNG),[1] helical pitches are 7.430 and 9.034 Å for the N- and Cl-springs, respectively. Figures 1 and 2 shows two springs in the unit cell, projected onto the XY plane. For a better understanding, atoms lying outside two helical strands were translated by proper lattice vectors. The figure also shows our convention for the atomic serial numbers to be used afterward. For each of the springs, a strand on the left-hand side constitutes a left-handed helix, while the one on the right-hand side forms a right-handed helix. In JUNG data for the N-spring, N42 and N44 of the N-spring are located above N45 and N46 by 5.685 and 5.460 Å along the helical axis, respectively. For the Cl-spring, N34 and N39 are located above N4 and N35 by 6.782 Å.

We first consider the geometry of the N-spring, which was optimized for a crystal whose cell parameters are the same as in JUNG. As summarized in Table 1, there are three major differences between the JUNG and PBE-OPT: (i) In the latter, the C−H bond lengths l(C−H) (1.08 Å) are in good agreement with those experimentally reported for aromatic compounds (1.084 Å).[14] As is known well, JUNG bond lengths (= 0.93 Å) show large discrepancies from the experimental data. Unexpectedly, LDA-OPT predicts bond lengths slightly longer than the experimental data. (ii) In PBE-OPT, interatomic distances between proximal silver atoms, Ag1−Ag28 and Ag27−Ag29 of 3.17 Å, are smaller than those in JUNG by 0.18 Å, which results in distances increased by more than 0.09 Å between silver atoms belonging to the same helical strands, l(Ag1−Ag27) and l(Ag28−Ag29). A similar behavior is also observed in LDA-OPT. In fact, these distances are smaller than the sum of the van der Waals radii[15] (3.40 Å) for a pair of silver atoms. However, we note that an Ag−Ag distance comparable to this value (3.227 Å) is also observed in the crystal structure of silver−pyridine complex in absence of any bridging ligation.[16] In addition, Ag−Ag distances in the coordination compounds are often found to be similar to those in the silver metal (2.89 Å).[17] One of possible explanations of this closed-shell $d^{10}-d^{10}$ interaction was given in terms of $s-d$ mixing. Relativistic effect are also nonnegligible,[18] but they are implicitly included in our calculations, since the pseudopotential of silver was generated from the scalar-relativistic all-electron atomic calculations.[19] (iii) Values of l(N−O) in NO_3^- groups (1.27 Å) are slightly longer than the average experimental data (1.24 Å[20] and 1.26 Å[21])

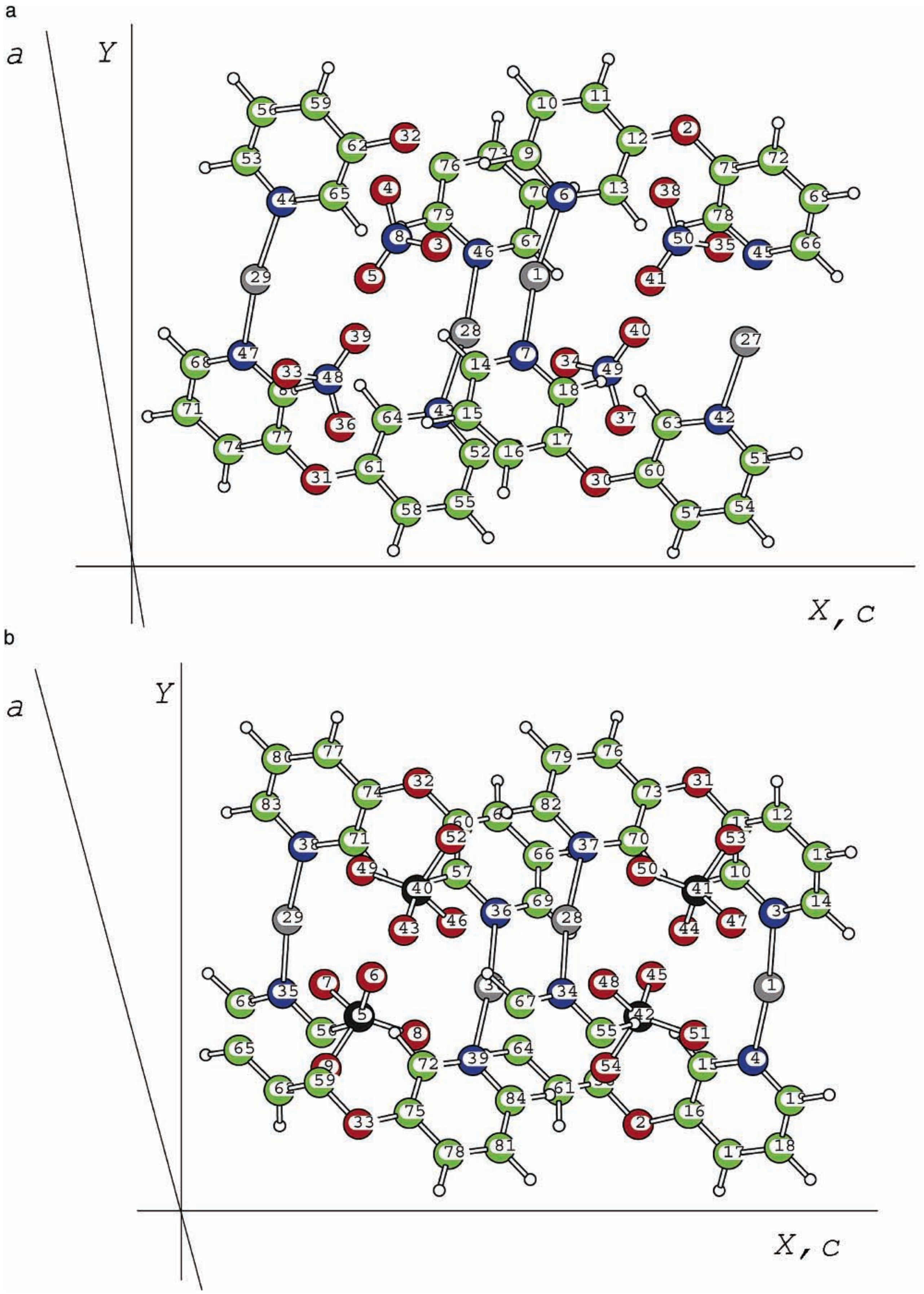

Figure 1. Structures of (a) N- and (b) Cl-springs projected onto XY planes. The *X* axis is parallel to the *c* axis and the *Z* axis to the *b* axis of the space group $P2_1/c$. The lattice vector **a** lies in the XY plane and makes an angle β with the *X* axis. Atoms lying outside the two helices were translated by proper lattice vectors. The numbering convention for atoms other than hydrogen is also shown. Different kinds of atoms are represented by different colors: green = carbon, blue = nitrogen, red = oxygen,, white = hydrogen, gray = silver, and black = chlorine.

TABLE 2: Bond Lengths (in Angstroms), Bond Angles, and Other Geometrical Parameters for the Cl-Spring[a]

	EXP	MP2	JUNG	LDA+0	PBE−5	PBE+0	PBE+5
l(C−H)	1.084		0.94(3)	1.10(1)	1.09(1)	1.09(1)	1.08(1)
l(Ag−Ag)[c]			3.36(0)	3.54(2)	3.40(1)	3.57(3)	3.96(1)
l(Ag−N)		2.241[d]	2.15(1)	2.17(1)	2.16(1)	2.18(1)	2.16(1)
l(Cl−O)	1.48[e]	1.490[f]	1.39(3)	1.45(1)	1.47(1)	1.47(1)	1.47(1)
l(N−N)[g]			4.29(0)	4.33(1)	4.30(1)	4.34(1)	4.28(1)
θ(N−N-X)[h]			81.9(0)	82.1(2)	81.5(2)	82.1(2)	81.8(3)
θ(N−Ag−N)[i]		180.0[d]	172.8(0)	174.7(9)	170.7(3)	174.6(9)	165.3(7)
θ(ion-ion-X)[j]			66.3(0)	63.7(4)	64.9(1)	63.5(4)	66.1(1)
χ[k]			63.7(0)	61.2(1)	63.6(2)	61.4(2)	64.2(7)

[a] EXP denotes values taken from experimental data, and MP2 represents data calculated in this work using the MP2 method in the GAUSSIAN98 program. JUNG denotes Jung et al's X-ray data at the lattice angle $\beta = 106.7°$. Other data were obtained in this work after structure optimization. LDA is based on the LDA parametrization due to Perdew and Zunger, while PBE denotes the GGA parametrization of ref 8. Suffixes −5, +0, and +5 correspond to $\beta = 101.7°, 106.7°$, and $111.7°$, respectively. Values in parentheses denote the standard deviations in the last decimal place. [b] Experimental data taken from ref 14. [c] Interatomic distance between proximal silver atoms not belonging to the same helical strand. [d] Value obtained in this work from a MP2/LANL2DZ calculation for the $Ag(NH_3)_2^+$ ion using the GAUSSIAN98 program. See caption d of Table 1 for more details. [e] Experimental data taken from ref 20. [f] Value obtained in this work from a MP2/6-31++G* calculation for ClO_4^- ion using the GAUSSIAN98 program. [g] Interatomic distance between nitrogen atoms belonging to the same N−Ag−N motif. [h] Angle that the N→N vector between nitrogen atoms in the same N−Ag−N motif makes with the *X* axis. [i] Bond angle between corresponding atoms in the same N−Ag−N motif. [j] Angle that the vector $ClO_4^- \rightarrow ClO_4^-$ between chlorate ions in the same helical strand makes with the *X* axis. [k] Angle that two N→N vectors in the same helical strand make with each other.

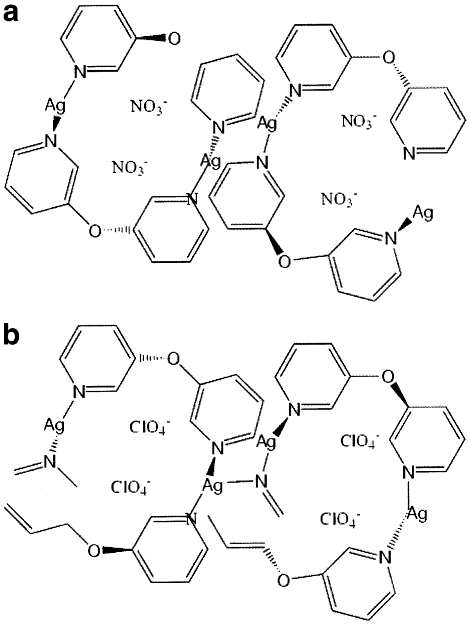

Figure 2. Schematic representations of (a) N- and (b) Cl-springs shown in Figure 1.

observed in the presence of various counterions. To make additional comparisons, we have performed a separate geometry optimization for the NO_3^- ion using the GAUSSIAN98 program.[22] A MP2 calculation with 6-31++G* basis set gives *l*(N−O)= 1.273 Å, which is in a very good agreement with that of PBE-OPT. On the other hand, the bond lengths in JUNG (1.22 Å) are much shorter than the MP2 value. Our additional calculation shows that LDA-OPT gives bond lengths that are in close agreement with those of PBE-OPT and MP2.

We also list two other differences between PBE-OPT and JUNG. (i) θ(N−Ag−N), the angle between atoms belonging to the same N−Ag−N motif, is smaller in PBE-PT than in the JUNG by approximately 3°, while the N−N distance in the motif is slightly longer. (ii) the angles χ, which two N−Ag−N motives belonging to the same helical strand make with respect to each other, are smaller by 1.6°. There are two such angles, the first one being defined by the vectors N6→N7 and N42→N45, and the second by N47→N44 and N46→N43. All these structural adjustments are accompanied by a marginal change in the angle θ(N−N-X) that the *X* axis makes with the vectors N47→N44, N43→N46, N7→N6, and N42→N45.

Next, we describe the major structural differences between JUNG and PBE-OPT for the Cl-spring whose lattice parameters are the same as in JUNG (see Table 2). (i) We again observe that C−H bond lengths (0.94 Å) are too short in JUNG, while those (1.09 Å) of PBE-OPT are in very good agreement with experimental data for those in the aromatic compounds. (ii) Contrary to the case of the N-spring, the interatomic distances of 3.57 Å between the proximal silver atoms (Ag1−Ag29, Ag28−Ag30) are larger than those in JUNG (3.36 Å) by more than 6%, which is manifested in smaller distances between Ag1−Ag28 and Ag29−Ag30. A similar behavior is observed in the LDA-OPT. (iii) We also note that there is a large difference in the two Cl−O bond lengths *l*(Cl−O) = (1.39 Å, 1.47 Å) between JUNG and PBE-OPT. The latter shows good agreement with experimental data reported for the ClO_4^- ion (1.48 Å). We have again performed a MP2 geometry optimization using the GAUSSIAN98 program for the isolated ClO_4^- ion, which resulted in *l*(Cl−O) = 1.490 Å. In JUNG, the bond lengths are smaller than the experimental and the MP2 data by more than 5%. Moreover, there is a large variation among them, three times larger than that in PBE-OPT (see Table 2). Turning to LDA-OPT, the bond lengths are slightly shorter than those in PBE-OPT. Contrary to the case of the N-spring, a slightly larger angle is observed for θ(N−Ag−N) in PBE-OPT than in JUNG. Similarly to the N-spring, the reverse is true for χ angles.

Change of Structure upon Deformation: Next, we describe the structural changes occurring upon deformation of the unit cell. To investigate these effects, we have optimized the geometry of the springs through a series of energy minimizations at different lattice angles. We first consider the N-spring. Optimizations were performed at two β angles (94.04° and 104.04°) apart from that observed in the X-ray structure (99.04°). All the other lattice parameters were the same. For simplicity, the parameter **a** was chosen to satisfy the relation $a(\sin\beta) = a_0(\sin\beta_0)$,where the subscript “0” denotes the quantities taken from the X-ray data. This corresponds to an application of a shear force along either the −X or +X directions. The important structural changes are as follows: (i) the vectors N47→N44, N43→N46, N7→N6, and N42→N45 tend to align more perpendicularly to the *X* axis at a larger β angle. In Table 1, this is easily seen from an increase of θ(N−N−X) upon an

TABLE 3: Angles that the N→O Vectors in the NO$_3^-$ Groups of the N-Spring Make with the *X* Axis[a]

	JUNG	LDA+0	PBE−5	PBE+0	PBE+5
N8−O3	−9.4	−9.8	−9.6	−9.9	−13.5
N8−O4	105.2	103.4	104.5	103.3	100.6
N8−O5	−125.8	−124.2	−126.3	−124.0	−128.3
N48−O33	170.6	170.8	172.6	170.8	170.5
N48−O36	−74.8	−75.4	−73.6	−75.3	−75.8
N48−O39	54.2	55.5	57.6	55.5	56.0
N50−O35	−9.4	−10.6	−9.7	−10.4	−15.0
N50−O38	105.2	105.4	106.3	105.3	101.8
N50−O41	−125.8	−124.5	−123.3	−124.6	−128.5
N49−O34	170.6	169.5	170.5	169.8	168.2
N49−O37	−74.8	−74.0	−73.2	−74.4	−75.9
N49−O40	54.2	55.4	56.9	55.4	54.0

[a] The notation is the same as that in Table 1.

TABLE 4: Angles that Cl→O Vectors in the ClO$_4^-$ Groups of the Cl-Spring Make with the *X* Axis[a]

	JUNG	LDA+0	PBE−5	PBE+0	PBE+5
Cl5−C6	73.2	73.0	75.2	73.4	78.0
Cl5−O7	140.2	148.8	139.2	148.7	141.1
Cl5−O8	−24.0	−6.1	−18.5	−5.7	−20.0
Cl5−O9	−124.8	−109.1	−122.3	−109.0	−123.9
Cl40−O43	−106.8	−105.2	−106.5	−104.9	−102.2
Cl40−O46	−39.8	−28.9	−46.4	−28.9	−29.8
Cl40−O49	156.0	176.9	160.6	177.4	163.5
Cl40−O52	55.2	73.5	55.5	73.8	61.9
Cl41−O44	−106.8	−107.5	−109.1	−107.4	−101.8
Cl41−O47	−39.8	−31.0	−46.4	−31.1	−30.3
Cl41−O50	156.0	174.6	160.2	174.9	166.5
Cl41−O53	55.2	71.5	55.6	71.8	63.6
Cl42−O45	73.2	72.6	72.2	72.5	73.3
Cl42−O48	140.2	149.4	141.2	149.4	137.5
Cl42−O51	−24.0	−20.5	−19.7	−20.7	−20.1
Cl42−O54	−124.8	−119.5	−122.0	−119.7	−123.5

[a] The notation is the same as that in Table 2.

increase of β . However, this increase (1.0°) is much smaller than that of β (10°). In addition, noticeable changes are induced in the N−N distance upon the change of β . This distance first increases from 4.28 to 4.30 Å as β increases from 94.04° to 99.04°, but it decreases to 4.25 Å as the angle increases by another 5°. This behavior is mostly due to the change of the Y component of the N→N vectors upon the change of the angle. Similar behavior is observed for the Ag−N bond lengths. (ii) Table 3 shows that oxygen atoms in NO$_3^-$ groups rotate clockwise in a concerted way as β increases, with the average rotation being 3.2° upon a 10° increase in β. Eleven out of 12 oxygen atoms turn out to rotate in the same direction in both of the first and the second increases of β by 5°. This is unexpected, since one could suppose that they would make a substantial counterclockwise rotation in accordance with the increase in β . No appreciable change is observed for the N−O bond length upon rotation (see Table 1). (iii) We observe that the relative displacements of NO$_3^-$ groups in the same helical strand, the vectors N48→N8 and N49→N50, tend to align more in parallel with the *Y* axis at a larger β angle. Again, this is mostly achieved by displacements (>0.1 Å) of N8 and N50 along +*Y* axis. (iv) As the β angle increases, silver atoms belonging to different strands come closer and distance between them reaches 3.17 Å at $\beta = 104.04°$. As we have already noted, this is still larger than the interatomic distances in the silver metal.

Calculations of total energy for the PBE-OPT at different β angles show that the equilibrium is located at an angle close to that observed in the X-ray structure. Furthermore, a simple calculation based on the harmonic approximation shows that the shear modulus is ∼0.01TPa, lying between those of lead and glass.[23] The total energy of a spring can be simply written as a sum of the kinetic energy of electrons E_{kin}, the electrostatic energy of ions and electrons E_{ES}, and the exchange−correlation energy E_{XC}. Our calculations give (ΔE_{tot}, $\Delta E_{\mathrm{kin}} + \Delta E_{\mathrm{ES}}$, ΔE_{XC}) = (0.023, 0.086, −0.063) and (0.019, 0.041, −0.022) at $\beta =$ 94.05° and 104.05°, respectively. Here, the energy differences Δ(in Hartree units) are calculated with respect to those at the X-ray β angle (=99.04°). We find that the sum of the kinetic and electrostatic energies strongly favors the X-ray angle, while the exchange-correlation partially compensates for large increases of these energies upon deformation. The differences in $E_{\mathrm{kin}}+E_{\mathrm{ES}}$ at different β angles can be largely ascribed to concurrent displacements of a large number of valence electrons around charged ions as the ions are moved. This can be seen by further decomposing E_{ES} into E_{ion} and the remaining contributions, where E_{ion} denotes the electrostatic energy of ion cores in interaction with other ion cores. We find very small increases in E_{ion} upon deformation. Namely, ΔE_{ion} = (0.003, 0.007) at β = 94.05° and 104.05°, respectively. Therefore, observed change in $E_{\mathrm{kin}}+E_{\mathrm{ES}}$ mainly originates from the redistribution of electron density around ion cores upon deformation, not by ionic displacements themselves.

Next, we consider deformations of the Cl-spring. Geometry optimization was performed at two other β angles (101.7° and 111.7°) in addition to that observed in the X-ray structure (106.7°). In general, the structural changes are more complicated than those of the N-spring. The important features can be summarized as follows: (i) The N−N vectors between nitrogen atoms belonging to the same N−Ag−N motifs tend to rotate counterclockwise by 0.6° upon the initial increase of β by 5° from 101.7°. However, these motifs are quite resistive to further rotation in the same direction. Instead, they exhibit a small clockwise rotation upon the increase of β to 111.7°. The change in θ(N−Ag−N) is consistent with this trend, since that angle also first increases and then decreases upon increases in β . (ii) On the average, the oxygen atoms in ClO$_4^-$ groups make large counterclockwise rotations of 9.1° upon the first increase. Fourteen of the 16 oxygen atoms rotate in the same direction (see Table 4), and this angle change is much larger than the one observed for the N-spring. A further increase in β induces an average clockwise rotation by 5.1°, but it is much less concerted because only 10 of them rotate in the same direction. (iii) Unexpectedly, the vectors Cl5→Cl40 and Cl42→Cl41 do not make an appreciable change in their angle with the *X* axis upon increase of β from 101.7° to 106.7°. However, an additional increase of the angle brings about counterclockwise rotations of the vectors by 2.6°, which are accompanied by relative displacements greater than 0.1 Å of Cl40 and Cl41 along the +*Y* axis. (iv) Unlike the case of the N-spring, the vectors between the proximal silver atoms, Ag30→Ag28 and Ag1→Ag29, get elongated as β increases. This is achieved by elongation along the *Z* axis, which can occur relatively easily due to the longer helical pitch of the Cl-spring.

Figure 3 shows a plot of the total energy as a function of β, which demonstrates that the equilibrium is located near $\beta =$ 106.7°. However, the curve has a strongly asymmetric form and it is more difficult to increase β than to decrease it. To make this point more clear, we made an additional calculation of the total energy for an optimized structure at $\beta = 99.2°$, for which we find that its energy is still lower than that at $\beta = 111.7°$. Compared to the N-spring, this spring is approximately twice as resistive to the increase of β by 5°, while it is 3 times softer with respect to its decrease. Similarly to the N-spring, separation of the total energy into its E_{ES}, E_{kin}, and E_{XC} components shows

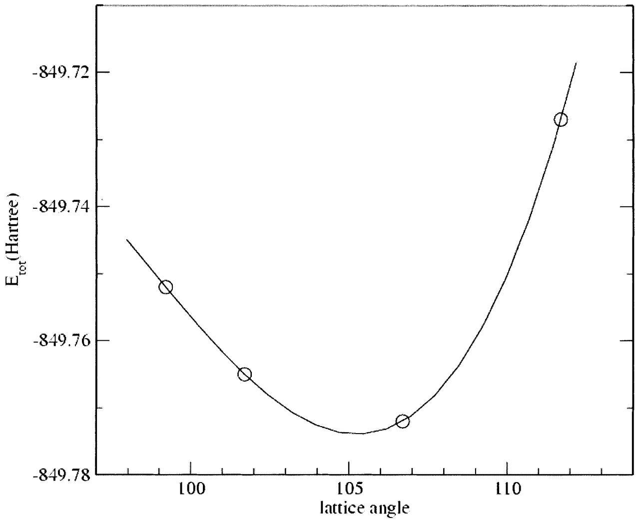

Figure 3. Total energy of the Cl-spring vs the lattice angle β: Open circles denote data points corresponding to PBE-OPT, while the solid line represents a cubic fit to those data.

that the stabilization of the X-ray β angle is due to the kinetic energy and the electrostatic contributions. Upon deformation, a large increase is induced in these components of the energy, which is only partly compensated for by the exchange-correlation contributions. Compared to total increases of $E_{\mathrm{kin}} + E_{\mathrm{ES}}$, we also observe very small increases in its ionic component E_{ion} upon deformation.

Electronic Density of States: Calculations of the electronic density of states (DOS) show that both N- and Cl-springs are semiconductors with calculated band gaps of about 2.45 and 2.39 eV, respectively. Since both GGA and LDA calculations substantially underestimate band gaps for most systems, the true band gaps are likely to be even larger. Figure 4 shows that the electronic densities of the N- and Cl-springs are quite similar to each other for both the valence and the conduction bands. We have also performed additional calculations of the DOS with lattice parameters $a = 18.368$ and 17.588 Å for the N- and Cl-springs, respectively. The supercell geometries in these calculations effectively correspond to those of two-dimensional crystals in which the periodicity along the lattice vector **a** is removed, since there is now a thick vacuum layer (>7.0 Å) along that axis. For these systems, there are substantial decreases in the normalized DOS due to the increased cell volumes. However, there are no significant changes in the band gaps (2.25 and 2.35 eV for the N- and Cl-springs, respectively). Noting that the periodicity along the lattice vectors ***a*** nor ***c*** cannot be due to covalent interactions, it is likely that the calculations for one-dimensional springs with periodicity only along the lattice vector **b** would also result in band gaps not much different from those in the two- and three-dimensional cases, suggesting that the band gap is mainly determined by interactions along the helical axis.

Conclusions

We have performed structural investigations of the monoclinic crystals of N- and Cl-molecular springs using real-space density functional calculations with generalized gradient approximation and also within the local density approximation. Some complementary MP2 calculations were also carried out. In comparison to Jung et al's X-ray data, the coordinates of the hydrogen and silver atoms, as well as those of the negative balancers, were refined through geometry optimization. Our calculations of the total energies as functions of the nonorthogonal lattice angle β correctly lead to minima near the experimentally observed values. In addition, we have investigated the elastic responses of the springs to changes in β, which lead to interesting structural changes. For the N-spring, nitrate ions make concerted rotations in a clockwise direction as the angle increases from 94.04° to 104.04° around the X-ray data value. For the Cl-spring, chlorate ions exhibit an enhanced rotation in the counterclockwise direction upon the increase of β from 101.7° to the X-ray value of 106.7°. However, they are quite resistive to further rotation in this direction, and an additional 5° increase leads to a rotation in the clockwise direction. These behaviors are strongly reflected in the shapes of the potential energy curves as a function of β. For the N-spring, the curve has a symmetric form, from which the shear modulus was estimated to be about 0.01TPa. For the Cl-spring, the curve is strongly asymmetric and shows that the spring is quite soft with respect to the decrease of β from the experimental value, while being much harder with respect to its increase. Calculations of electronic density of states reveal that both springs are medium gap semiconductors.

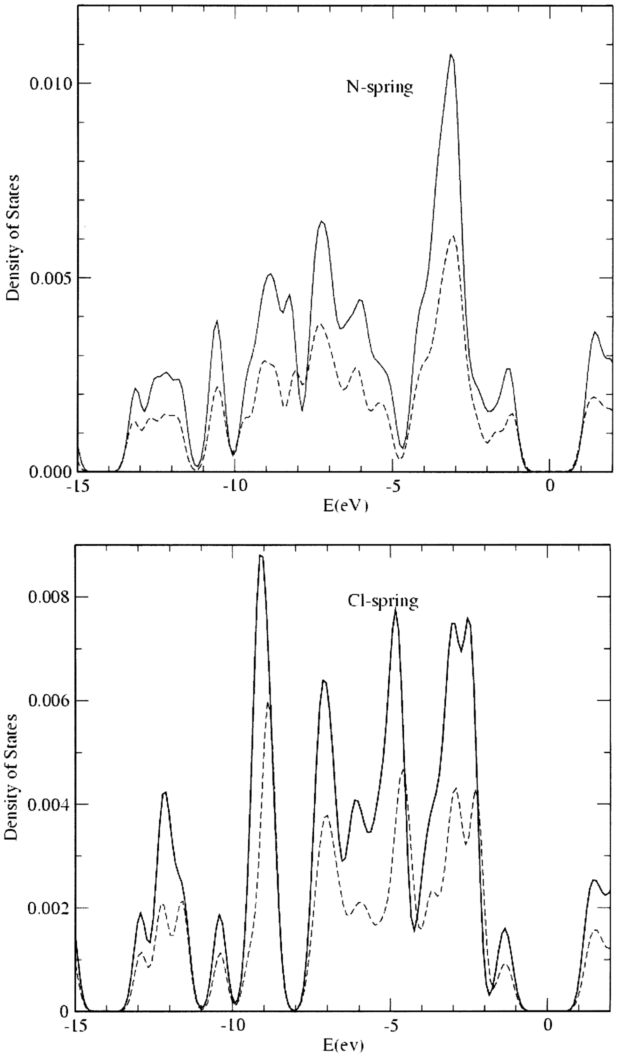

Figure 4. Electronic density of states for (a) the N- and (b) Cl-springs for the PBE-OPT. In each case, the Fermi level is at zero of the energy axis. Solid lines correspond to the three-dimensional crystals, while dashed lines represent the two-dimensional ones. See the text for more details.

Acknowledgment. Hong Seok Kang thanks Jeonju University for financial support during a sabbatical leave. We also appreciate the North Carolina Supercomputing Center and the supercomputer center at Chonbuk National University for their computational supports.

Supporting Information Available: Cartesian coordinates for the optimized structures obtained from the PBE calculations for the N- and Cl-springs at different lattice angles, and the corresponding data from the LDA calculation at the lattice angles given in the X-ray data. This material is available free of charge via the Internet at http://pubs.acs.org.

References and Notes

(1) Jung, O.-S.; Kim, Y. J.; Lee, Y.-A.; Park, J. K.; Chae, H. K. *J. Am. Chem. Soc.* **2000**, *122*, 9921.

(2) Dreizler, R. M.; Gross, E. K. U. *Density Functional Theory*; Springer: Berlin, 1990.

(3) Ashcroft, N. W.; Mermin, N. D. *Solid State Physics*; Holt, Rinehart and Winston: New York, 1976; Chapter 11.

(4) Briggs, E. L.; Sullivan, D. J.; Bernholc, J. *Phys. Rev. B* **1996**, *54*, 14362.

(5) Kleinman, L.; Bylander, D. M. *Phys. Rev. Lett.* **1982**, *48*, 1425.

(6) Troullier, N.; Martins, J. L. *Phys. Rev. B.* **1991**, *43*, 1993.

(7) Bachelet, G. B.; Hamann, D. R.; Schlüter, M. *Phys. Rev. B* **1982**, *26*, 4199.

(8) Perdew, J. P.; Burke, K.; Ernzerhof, M. *Phys. Rev. Lett.* **1996**, *77*, 3865.

(9) Brandt, A. *Math. Comput.* **1977**, *31*, 333; *GMD Studien* **1984**, *85*, 1.

(10) (a) Buongiorno Nardelli, M.; Yakobson, B. I.; Bernholc, J. *Phys. Rev. B* **1998** *57*, R4277. (b) Zhao, Q.; Buongiorno Nardelli, M.; Bernholc, J. *Phys. Rev. B* **2002** *65*, 144105. (c) Buongiorno Nardelli, M.; Fattebert, J.-L.; Bernholc, J. *Phys. Rev. B* **2001** *64*, 245423.

(11) Schmidt, W. G.; Briggs, E. L.; Bernholc, J. Bechstedt, F. *Phys. Rev. B* **1999** *59*, 2234; Lu, W.; Schmidt, W. G.; Briggs, E. L.; Bernholc, J. *Phys. Rev. Lett.* **2000** *85*, 4381; Boguslawski, P.; Bernholc, J.; *Phys. Rev. Lett.* **2002** *88*, 166101.

(12) (a) Hellmann, H. In *Einführung in die Quantumchemie*; Deuticke: Leipzig, 1937. (b) Feynman, R. P. *Phys. Rev.* **1939**, *56*, 340.

(13) Perdew, J. P.; Zunger, A. *Phys. Rev. B* **1981**, *23*, 5048.

(14) *CRC Handbook of Chemistry and Physics*, 61st ed.; Weast, R. C., Ed.; CRC Press: Boca Raton, FL, 1980; p F218.

(15) Huheey, J. E. In *Inorganic Chemistry*, 2nd ed.; Haper & Row: New York, 1978; p 232.

(16) Singh, K.; Long, J. R.; Stavropoulos, P. *J. Am. Chem. Soc*. **1997**, *119*, 2942.

(17) Jansen, M. *Angew. Chem.*, *Int. Ed. Engl.* **1987**, *26*, 1098.

(18) Pykkö, P. *Chem. Rev.* **1988**, *88*, 563.

(19) (a) Koelling, D. D.; Harmon, B. N. *J. Phys. C.* **1977**, *10*, 3107. (b) Fuchs, M.; Scheffler, M. *Comput. Phys. Commun.* **1999**, *119*, 67.

(20) Lindin, R. A.; Andreeva, L. L.; Molochko, V. A. In *Constants of Inorganic Substances*: *A Handbook*; Lidin, R. A., Ed.; Begel House: New York, 1995; p 207.

(21) Gillespie, R.; Humphreys, D. A.; Baird, N. C.; Robinson, E. A. In *Chemistry*; Allyn and Bacon: Boston, 1986; p 636.

(22) Frisch, M. J.; Trucks, G. W.; Schlegel, H. B.; Scuseria, G. E.; Robb, M. A.; Cheeseman, J. R.; Zakrzewski, V. G.; Montgomery, J. A., Jr.; Stratmann, R. E.; Burant, J. C.; Dapprich, S.; Millam, J. M.; Daniels, A. D.; Kudin, K. N.; Strain, M. C.; Farkas, O.; Tomasi, J.; Barone, V.; Cossi, M.; Cammi, R.; Mennucci, B.; Pomelli, C.; Adamo, C.; Clifford, S.; Ochterski, J.; Petersson, G. A.; Ayala, P. Y.; Cui, Q.; Morokuma, K.; Salvador, P.; Dannenberg, J. J.; Malick, D. K.; Rabuck, A. D.; Raghavachari, K.; Foresman, J. B.; Cioslowski, J.; Ortiz, J. V.; Baboul, A. G.; Stefanov, B. B.; Liu, G.; Liashenko, A.; Piskorz, P.; Komaromi, I.; Gomperts, R.; Martin, R. L.; Fox, D. J.; Keith, T.; Al-Laham, M. A.; Peng, C. Y.; Nanayakkara, A.; Challacombe, M.; Gill, P. M. W.; Johnson, B.; Chen, W.; Wong, M. W.; Andres, J. L.; Gonzalez, C.; Head-Gordon, M.; Replogle, E. S.; Pople, J. A. GAUSSIAN98, revision A.11; Gaussian, Inc.: Pittsburgh, PA, 2001.

(23) Sears, F. W.; Zemansky, M. W. In *University Physics*; Addison-Wesley Publishing Co.: London, 1970; p 155.